Kaminsky, F., Wirth, R., Matsyuk, S., Schreiber, A., Thomas, R. (2009): Nyerereite and nahcolite inclusions in diamond: evidence for lower-mantle carbonatitic magmas. - *Mineralogical Magazine*, *73*, 5, 797-816

DOI: 10.1180/minmag.2009.073.5.797

Mineralogical Magazine, October 2009, Vol. 73(5), pp. 797–816

Nyerereite and nahcolite inclusions in diamond: evidence for lower-mantle carbonatitic magmas

F. KAMINSKY[1,*], R. WIRTH[2], S. MATSYUK[3], A. SCHREIBER[2] AND R. THOMAS[2]

[1] KM Diamond Exploration Ltd., 2446 Shadoldt Lane, West Vancouver V7S3J1, British Columbia, Canada
[2] Helmholtz Centre Potsdam GFZ German Research Centre for Geosciences, Experimental Geochemistry and Mineral Physics, Telegrafenberg, D14473 Potsdam, Germany
[3] Institute of Gechemistry, Mineralogy and Ore Formation, National Academy of Sciences of Ukraine, Palladin Av., 03680 Kyiv-142, Ukraine

[*Received 17 March 2009; Accepted 27 August 2009*]

ABSTRACT

Nyerereite and nahcolite have been identified as micro- and nano-inclusions in diamond from the Juina area, Brazil. Alongside them are Sr- and Ba-bearing calcite minerals from the periclase-wüstite series, wollastonite II (high), Ca-rich garnet, spinels, olivine, phlogopite and apatite. Minerals of the periclase-wüstite series belong to two separate groups: wüstite and Mg-wüstite with Mg# = 1.9–15.3, and Fe-periclase and periclase with Mg# = 84.9–92.1. Wollastonite-II (high, with Ca:Si = 0.992) has a triclinic structure. Two types of spinel were distinguished among mineral inclusions in diamond: zoned magnesioferrite (with Mg# varying from 13.5–90.8, core to rim) and Fe spinel (magnetite). Olivine (Mg# = 93.6), intergrown with nyerereite, forms an elongate, lath-shaped crystal and most likely represents a retrograde transformation of ringwoodite or wadsleyite. All inclusions are composed of poly-mineralic solid mineral phases. Together with previously found halides, sulphates and other mineral inclusions in diamond from Juina, they form a carbonatitic-type mineral paragenesis in diamond which may have originated in the lower mantle and/or transition zone. Wüstite inclusions with Mg# = 1.9–3.4, according to experimental data, may have formed in the lowermost mantle. The source for the observed carbonatitic-type mineral association in diamond is lower-mantle natrocarbonatitic magma. This magma may represent a juvenile mantle melt, or be the result of low-degree partial melting of deeply-subducted carbonated oceanic crust. This magma was rich in volatiles, such as Cl, F and H, which played an important role in the formation of diamond.

KEYWORDS: diamond, inclusion, TEM, carbonates, halides, nyerereite, nahcolite, carbonatitic magma, lower mantle.

Introduction

AMONG upper-mantle mineral inclusions in diamond, two paragenetic associations, (1) ultramafic and (2) eclogitic are commonly distinguished. With the discovery of transition-zone and lower-mantle diamonds, these same two associations appeared to be present as inclusions, represented only by other mineral phases stable under higher pressure conditions: (1) ringwoodite (γ-olivine), majoritic garnet (in the transition zone, up to 660 km depth), Mg-Si perovskite and ferropericlase (in the lower mantle below 660 km) for the ultramafic association; and (2) 'phase Egg', stishovite (Wirth *et al*., 2007), and probably others for the eclogitic association. Recently, the authors have identified a series of halides, calcite, wollastonite II, anhydrite, phlogopite, cuspidine and other minerals as new inclusions in diamond (Wirth *et al*., 2009). Continuing these studies, we have now identified fresh, well preserved nyerereite and nahcolite, in association with other minerals, as inclusions in

* E-mail: felixvkaminsky@cs.com
DOI: 10.1180/minmag.2009.073.5.797

diamond crystals collected from the Rio Soriso placer deposit, which is located in the northwestern part of the Juina area, Mato Grosso State, Brazil. Alluvial placer deposits in the Juina area were extensively mined in the late 1980s–early 1990s producing, according to the local sources, up to 5–6 million carats of diamond each year. In 2006–2007, primary sources to these diamonds were discovered; they are early Cretaceous (93.6 Ma) kimberlitic pipes located within the Chapadão Plateau, at the head of a drainage system which has produced most of the alluvial diamonds mined in the Juina area (Kaminsky, *et al*., 2009*b*).

Nyerereite, a Na-K-Ca bicarbonate mineral $(Na,K)_2(Ca,Sr,Ba)(CO_3)_2$, was first identified in the early 1960s by J.B. Dawson in recently erupted natrocarbonatitic lavas and ashes of the Oldoinyo Lengai volcano in northern Tanzania (Dawson, 1962). Nyerereite is often calcified, reflecting its instability under atmospheric conditions. Nahcolite $NaHCO_3$, one of the intermediate products of hydration of nyerereite is widespread in altered natrocarbonatites, forming nests, veinlets and thin veins inside carbonatite flows.

It has been suggested that some pre-modern calcitic carbonatite lavas and pyroclastic material containing nyerereite, nahcolite and other Na-K-Ca carbonates, may have been erupted as alkali carbonatite but were subsequently leached of their alkalis and transformed into sövites (Dawson, 1993), and that natrocarbonatitic magma is in fact the primary magma for Ca- and F-rich carbonatites (Le Bas, 1981). Others have proposed that natrocarbonatite is a derivative of primary, Mg- or Ca-rich carbonatite melt (e.g. Gittins and Harmer, 1997) which may derive directly from the mantle.

In kimberlite, nyerereite occurs in chloride-carbonate clasts from the Udachnaya-East kimberlite pipe, Siberia, where it is associated with shortite, pirssonite, gaylussite, calcite, trona and andrasvumite (Kamenetsky *et al*., 2006; Sharygin *et al*., 2008). These clasts are of particular interest because some of them contain magmatic halides (principally halite and sylvite) within the groundmass (Kamenetsky *et al*., 2006). Zemkorite, initially described as a new carbonate, and further considered as a nyerereite isomorph (R. Mitchell, pers. comm.), was reported in kimberlites of the Udachnaya pipe, Siberia, Russia (Egorov *et al*., 1988), and within Pipe-7, Wajrakarur, South India (Parthasarathy *et al*., 2002).

In this work, we present the results of detailed, comprehensive studies of nyerereite, nahcolite and other minerals included in diamond, which, to date, do not belong to any known paragenetic association, and our interpretation of these findings.

Analytical techniques

Following on from our previous studies of diamonds from the Juina area (Kaminsky *et al*., 2001, 2009*a*; Wirth *et al*., 2007, 2009), we studied a new suite of samples from the Rio Soriso placer deposit. During the course of microscopic examination, one of the stones appeared to be particularly rich in mineral inclusions, including some minerals which have not previously been observed in diamond. This diamond (#8/103) was selected for a more detailed study.

Two IR spectra of diamond #8/103 were obtained from a flat, diamond plate with a thickness of 3.249 mm over the range of 400–4000 cm^{-1} utilizing a Bruker ISF 66v FTIR spectrometer attached to a Hyperion microscope coupled with an IRScope microscope and a KRS-5 polarizer at the GeoForschungsZentrum (GFZ) Potsdam. The resulting spectra were acquired from optically transparent parts of the diamond, with an aperture diameter of 60–90 μm and a spectral resolution of 2 cm^{-1}; the total number of scans was 256. Spectra were created in absorption units using *Opus ver. 5.5* software. The nitrogen content and its aggregation were calculated by applying the technique described in Taran *et al*. (2004).

For study of the inclusions, the diamond was cut into two parts by means of a laser. This permitted identification, in the interior of the diamond, of several small (micrometre-sized) mineral inclusions. Several electron transparent foils were milled from both parts of the diamond by focused-ion beam (FIB) techniques with a single beam device (FEI FIB 200 TEM) operated at GFZ Potsdam (Ga-ion beam, 30 keV acceleration voltage). The foil thickness varied from 100–120 nm. Details of the FIB method applied herein are presented in Wirth (2004).

The foils were studied at the GFZ Potsdam using transmission electron microscopy (TEM) methods, such as bright-field and dark-field imaging, high-angle annular dark-field imaging (HAADF), electron diffraction, electron energy-loss spectroscopy (EELS) and analytical electron microscopy (AEM), utilizing a TECNAI F20 XTWIN transmission electron microscope. The chemical composition of inclusions was measured

by AEM and EELS. It should be noted that chemical compositions of minerals, determined with the use of these techniques in at.%, are based not on determinations of each element concentration but on the peak intensity with an assumption that the total is equal to 100%. The AEM was performed with an X-ray analyser with an ultra-thin window. The X-ray intensity spectra were usually acquired in the scanning transmission mode (STEM) scanning the electron beam in a selected window ~20 nm × 20 nm in size (window analysis), thus reducing mass loss during the measurement significantly. It proved very difficult to study and identify the smallest of the mineral phases (some only 20–30 nm in size) because, due to the foil thickness (~100–120 nm), several small grains might be stacked on top of each other. Some of the phases discussed below were identified from high-resolution element maps evaluating the EDX spectra pixel by pixel.

Some inclusions were identified with the aid of Raman spectroscopy, which is a non-destructive, high-sensitivity technique requiring minimal sample volume and preparation (e.g. Thomas *et al*., 2008). Raman spectra were recorded at the GFZ Potsdam with a Jobin-Yvon LabRam HR800 spectrometer (grating: 1200 gr mm^{-1}), equipped with an Olympus optical microscope and a long-working-distance LMPlanFI 100 ×/0.80 objective. This has a lateral resolution of ~1 μm and a depth resolution of ~2 μm which allows for confocal spectral measurements from selected regions within mineral samples, and thus enables the characterization of mineral inclusions in the diamond host. We used a 514 nm excitation of a Coherent Ar^{+} laser (Model: Innova 70C), powered at 300 mW (about 45 mW on sample), at a resolution $\leqslant$0.6 cm^{-1}. Each unpolarized spectrum represents the accumulation of six acquisitions, each of 20 s duration. The spectra were collected at a constant laboratory temperature of 20ºC, with a Peltier-cooled CCD detector. The positions of the Raman bands were controlled and eventually corrected using the principal plasma lines in the Argon laser. The measured positions of the plasma lines in the fingerprint spectral region are not larger than 0.6 cm^{-1}.

Results

The host diamond

Diamond #8/103 is a typical dodecahedroid for the Juina area. Its dimensions are 5.2 mm × 4.9 mm × 3.8 mm. Optical microscopy reveals numerous inclusions of differing size and colour within the stone. The TEM study indicates its low dislocation density. The N concentration in diamond #8/103, detected with Fourier Transform Infrared Spectroscopy (FTIR) (Fig. 1), and consisting only of B-centres (N_B), is 44 ppm; i.e. this is a low-N Type IaB diamond. Such small concentration and high N aggregation ratios are characteristic for lower-mantle diamonds (e.g. Kaminsky *et al*., 2001). Another interesting feature of this stone, as for most lower-mantle diamonds in the Juina area, is a large concentration of the H impurity centre, identified at 3107 and 1405 cm^{-1} in the IR spectrum (Fig. 1). Commonly, this type of centre is either absent or weakly expressed. In contrast to the majority of diamond deposits worldwide, almost all diamonds from the Juina pipes (80–89%) have noticeable (up to 4.2 cm^{-1}) levels of the hydrogen C–H centre (Kaminsky *et al*., 2009*a*).

Inclusions in the diamond

Inclusions were identified in seven foils prepared from the first part of diamond #8/103: ##1622,

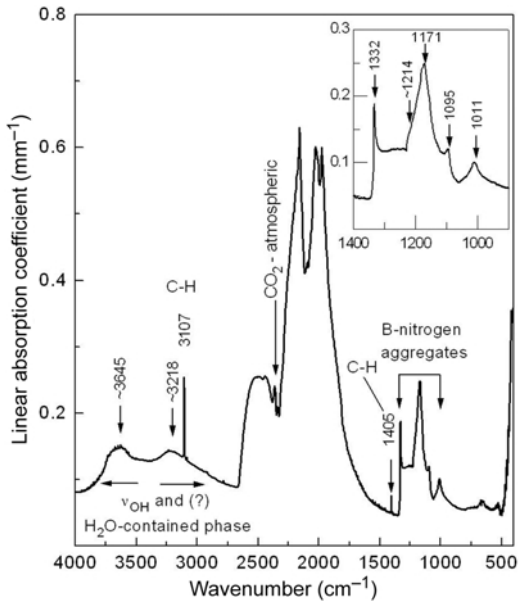

FIG. 1. Infrared spectrum of diamond #8/103 obtained from a plate with a thickness d = 3.249 mm, normalized to a thickness of 1 mm. Details of aggregated nitrogen B-centres, which dominate in the diamond, are presented in the insert. Note the high intensity of the C–H impurity centre marked at 3107 and 1045 cm^{-1}.

1625, 1658, 1659, 1671, 1673 and 1734 (Table 1). Inclusions are always composed of minerals of micron- to nanometre-size and, locally, non-crystalline material, and cavities that were filled with a fluid or gas phase prior to TEM sample preparation. During FIB sample preparation, a fluid (or gas) has been released. All inclusions are fully encapsulated within the diamond, i.e. they are not connected to the diamond surface. This proves that they are syngenetic to the diamond.

Depending upon the size of the inclusion, the mineral inclusions were recognized either as small, perfectly euhedral crystals (tiny nano-inclusions, smaller than the thickness of the foil) or two-dimensional plates (inclusions thicker than a foil), for which the habit could not be ascertained. All nanometre-sized inclusions were identified by their chemical composition, and some additionally by their calculated electron-diffraction pattern derived from high-resolution images (FFT). Micrometre-sized inclusions were routinely identified by their electron-diffraction pattern and chemical composition.

An interesting inclusion was found in foil #1734. In addition to a rhombic-shape, plate-like portion (~4 μm × 4 μm in size) composed of a calcite matrix with minor porosity and nano-inclusions of nyerereite, wollastonite II and

TABLE 1. List of mineral inclusions in diamond #8/103.

Foil #	Micro-inclusions	Nanometre-sized inclusions	Grain size	Method
1622	Plate-like inclusion, 500 nm wide	Fe-spinel (magnetite), 30–60 nm Porosity (~30%)	30–60 nm	TEM
1625	Plate-like inclusion, 1.5 μm × 1.0 μm Carbonate (calcite?) matrix,	Fe-periclase, periclase (Mg# = 84.9–92.1) Wüstite, Mg-wüstite (Mg# = 1.9–15.3) Porosity	100 nm 20–40 nm	TEM
1658	Plate-like inclusion, 1.5 μm wide Graphite matrix	Fe-spinel Porosity	30–100 nm	TEM
1659	Plate-like inclusion, 6 μm × 2.2 μm: Nyerereite, 4 μm × 1.5 μm Olivine (Mg# = 93.6), 2 μm × 0.25 μm	Magnesioferrite (Mg# = 12.0–78.4) Apatite Phlogopite (?)	300–700 nm 500 nm 350 nm	TEM
1671	Plate-like inclusion, 0.22 μm wide	Calcite (with Ba and Sr) Fe-spinel Apatite Mg-wüstite Porosity	 All <100 nm	TEM
1673	Plate-like inclusion, 4 μm × 0.55 μm	Calcite (with Sr) Mg-Fe spinel Phlogopite (?) Graphite Porosity	 All 200–300 nm >300 nm	TEM
1734	Rhombic-shape inclusion, 4 μm × 4 μm: Calcite (with Sr) matrix Appendage, 5 μm × 0.2 μm Nyerereite matrix	Nyerereite Wollastonite II (triclinic) Ca-garnet (Ca-Ti-Al-Mg-Fe-Zr) Diamond Calcite (with Sr) Apatite (La-, Ce-, Nd-enriched) Mg-wüstite (?) Porosity	500 nm × 1000 nm 200 nm × 500 nm 200 nm × 600 nm 250 nm × 350 nm <100 nm <100 nm	TEM
Second part of the stone	Nahcolite + calcite + phlogopite (5–10 μm)			Raman

Ca-rich garnet (Fig. 2*a*), it has an 'appendage'. The 'appendage' is a fissure-like feature, ~5 μm by 150–200 nm (Fig. 2*b*). It begins at the nyerereitic corner of the main, plate-like part of the inclusion and ends within the host diamond; there is no connection between the 'appendage' and the diamond surface. The matrix of the 'appendage' is connected to the main micro-inclusion and has the same composition, i.e. nyerereite. It contains several nano-crystals of differing chemical composition and grain size (Fig. 2*c*). The average grain size of these nano-crystals is less than 50 nm; the largest grains are approximately 100 nm in size. Among the identified grains are calcite, apatite, wollastonite II (high), and a Fe-oxide phase (Mg-wüstite?). Another interesting feature is the inclusion of diamond within the main, plate-like portion (Fig. 2*d*); it is described in detail later in the text.

The second part of diamond crystal #8/103 was studied with the aid of Raman microspectroscopy. The Raman spectra, acquired from inclusions in this part of the diamond, show the presence of nahcolite, calcite and phlogopite.

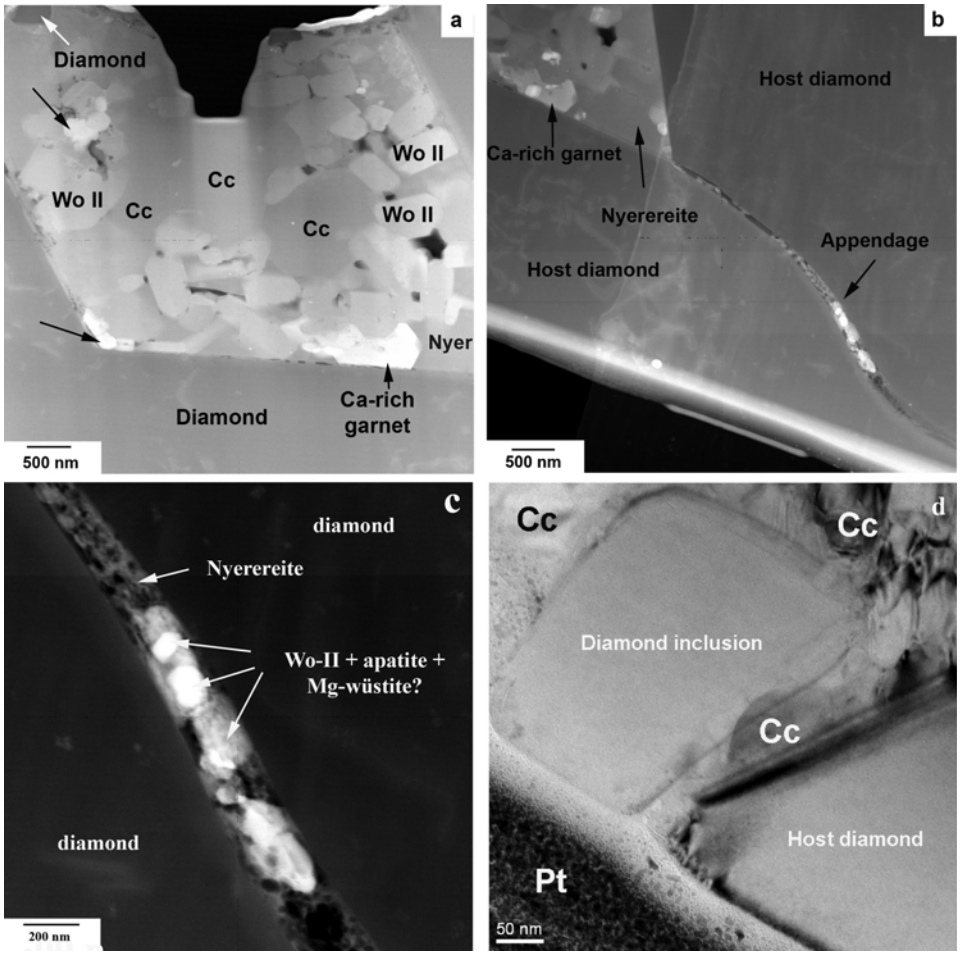

FIG. 2. HAADF images of polymineralic inclusion in diamond; foil #1734. (*a*) Major, plate-like part of the inclusion composed of calcite (Cc), wollastonite II (Wo II), nyerereite (Nyer), Ca-rich garnet (black arrows), and diamond. The darker spot-like contrast, especially between the Wo II grains displays nano-pores. (*b*) An 'appendage', composed of nyerereite with nano-inclusions of apatite (rich in La, Ce, and Nd) and magnesiowüstite (?). (*c*) A detail of the 'appendage'. One can see an interference of different nanometric phases. (*d*) TEM bright field image of the diamond inclusion in carbonate matrix (Cc). Pt is the platinum strip from the FIB sample preparation.

Minerals present within the diamond-hosted inclusions

Carbonates

Carbonate micro- and nano-inclusions are represented by nyerereite, nahcolite and calcite. Nyerereite and nahcolite are herein identified as a mineral inclusion in diamond for the first time. Nyerereite has a 'touching' association in diamond with calcite, wollastonite II (high), apatite, Ca-rich garnet, olivine, spinel and, probably, phlogopite and magnesiowüstite. Nahcolite was found in diamond as a single-grain inclusion; calcite and phlogopite grains were identified in the close vicinity.

Nyerereite

Nyerereite is present in two different micro-inclusions. In foil #1734, nyerereite forms a euhedral inclusion in a matrix of calcite, and within the matrix of the 'appendage', where it is in association with calcite, apatite, wollastonite II (high), and wüstite (?) (Fig. 2). In foil #1659, nyerereite comprises the matrix of a micro-inclusion and forms a single crystal ~4 μm × 2 μm in size which is intergrown with olivine and which encapsulates nano-inclusions of spinel, apatite and phlogopite (?) (Fig. 3).

The chemical composition of nyerereite, measured by scanning the electron beam in a window of 200 nm × 300 nm in STEM mode using the EDX-system (Fig. 4), is presented in Table 2. High-resolution element mapping using the Na-$K\alpha$, K-$K\alpha$ and Ca-$K\alpha$ X-ray intensities demonstrates that the chemical composition of the crystal varies locally with respect to these elements.

Diffraction contrast, together with electron diffraction, demonstrates that the grain in foil #1659 is a single crystal. Diffraction patterns (Fast Fourier Transforms, FFT), calculated from high-resolution images of the mineral, were indexed, based on the hexagonal crystal structure of nyerereite (high) with the space group $P6_3mc$. The high-nyerereite structure is the aristotype for all phases in the system $Na_2Ca(CO_3)_2$–$K_2Ca(CO_3)_2$ with the exception of bütschliite (McKie and Frankis, 1976). Applying this crystal structure to the diffraction pattern data evaluation, the zone axis of the diffraction pattern is $[3\bar{1}\bar{1}]$ and the (hkl) planes identified are (clockwise): $(01\bar{1})$, $(\bar{1}1\bar{4})$, $(\bar{1}0\bar{3})$, $(\bar{1}\bar{1}\bar{2})$ and $(0\bar{1}1)$. The crucial

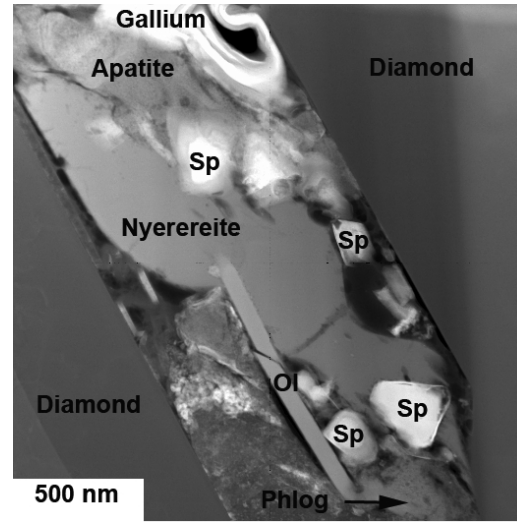

FIG. 3. HAADF image of a large single crystal of nyerereite intergrown with a lath-shaped olivine (Ol), several zoned spinel grains (Sp), apatite and phlogopite. Foil #1659.

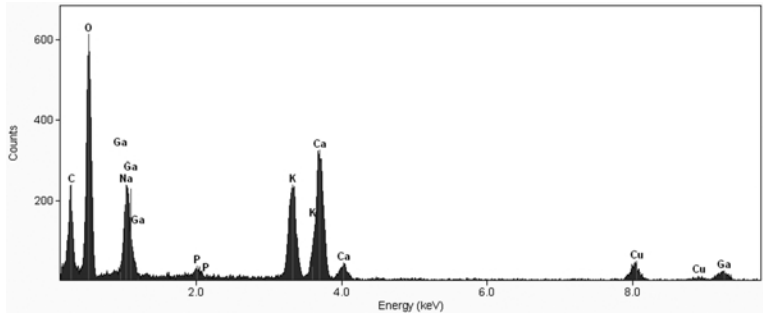

FIG. 4. EDX spectrum indicating the chemical composition of the nyerereite crystal from inclusion in foil #1659, displayed in Fig. 3.

TABLE 2. Chemical composition of nyerereite (EDX analysis).

Element	At.% Foil #1659	At.% Foil #1734	Oxide	Wt.% Foil #1659	Wt.% Foil #1734
Ca	36.5	37.8	CaO	20.6	21.8
Na	33.3	41.3	Na_2O	18.3	23.1
K	28.3	19.7	K_2O	13.8	10.0
Sr	n.d.	0.7	SrO	n.d.	0.15
P	1.9	0.5	P_2O_5	3.4	1.12
Total*	100.0	100.0	Total	56.1	56.17

* Carbon and O are also present in the spectrum but were not quantified because the mass absorption coefficients for C-*K*α and O-*K*α are not reliable, even if available or calculated.
n.d. = not detected.

test, as to whether the diffraction pattern is correctly indexed and thus conforms to the crystal structure, is the comparison of the observed angles between adjacent planes and the calculated angles. The observed results are in good agreement with the angles calculated for nyerereite (Table 3).

The compositions of the two analysed grains correspond well to nyerereite both from natrocarbonatitic lavas of Oldoinyo Lengai and from the segregations in Siberian kimberlites, having only a slightly smaller Ca content and an elevated K content (Table 4; Fig. 5).

Nahcolite

Nahcolite was identified in the second part of the diamond along with calcite and phlogopite. The Raman micro-spectrum, obtained from this inclusion, is presented in Fig. 6. It has two Raman bands at 684 $cm^{-1}$and 1046 cm^{-1} that are indicative of nahcolite (e.g. Hoshino *et al*., 2006).

TABLE 3. Comparison of the observed angles between adjacent planes and the calculated angles for nyerereite.

Angle between planes	Observed	Calculated
$(\bar{1}\bar{1}\bar{2}):(0\bar{1}1)$	50º	49.82º
$(\bar{1}\bar{1}\bar{2}):(\bar{1}0\bar{3})$	35º	34.38º
$(\bar{1}0\bar{3}):(0\bar{1}1)$	85º	84.20º
$(01\bar{1}):(\bar{1}0\bar{3})$	95º	95.80º
$(\bar{1}0\bar{3}):(\bar{1}1\bar{4})$	38º	38º
$(\bar{1}1\bar{4}):(01\bar{1})$	57º	57º

Calcite

Calcite was identified in three foils (##1671, 1673 and 1734), both as a polycrystalline matrix, with individual crystals ~1−2 μm in size (foil #1734, Fig. 2*a*), and as nano-inclusions of 100−300 nm in size (foils ##1671 and 1673). In some cases (foil #1625, Fig. 7*a*) the calcitic matrix was rendered amorphous due to the high-energy implantation of gallium ions during the course of FIB-milling (see next section).

Several isolated calcite crystals were identified additionally by Raman spectrometry in the other

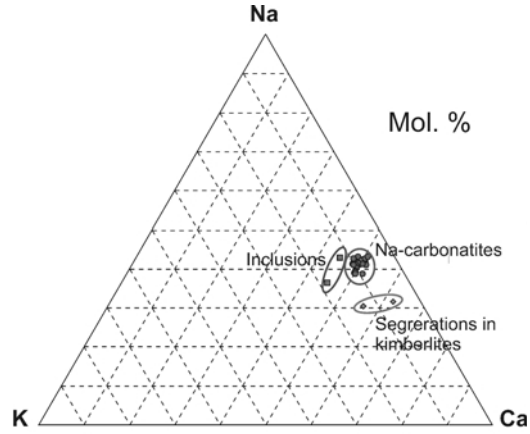

FIG. 5. Na-Ca-K composition diagram for nyerereite from different localities. Data on nyerereite from natrocarbonatites after Gittins and McKie (1980), Peterson (1990), Zaitsev and Chakhmouradian (2002), Mitchell (2006), Zaitsev *et al*. (2008*a*,*b*). Data on nyerereite from segregations in kimberlite after Kamenetsky *et al*. (2006).

TABLE 4. Comparative chemical characteristics of Na-K-Ca carbonates.

Characteristics	Inclusions in diamond, this work	Nyerereite		Gregoryite, Na-carbonatite***
		Na-carbonatite*	Segregations in kimberlite**	
Wt.%				
CaO	20.55–21.8	23.81–26.32	28.75–31.68	4.26–11.79
Na_2O	18.26–23.1	21.01–24.19	17.26–17.75	40.32–50.90
K_2O	10.0–13.78	4.74–9.05	5.19–11.43	1.97–4.31
Mol.%				
%CC, mol.	44.8–45.4	47.9–52.0	56.2–62.3	8.3–23.3
%NC	36.5–43.0	38.7–43.2	30.5–31.6	71.9–89.4
%KC	12.2–18.1	5.9–10.9	6.1–13.3	2.3–5.1
At. ratios				
Na/K	2.01–3.51	3.59–7.37	2.29–5.20	14.42–39.26
Na/Ca	1.61–1.92	1.49–1.79	1.01–1.09	6.19–17.04
(Na+K)/Ca	2.41–2.46	1.84–2.17	1.21–1.56	6.60–17.66

* after Gittins and McKie (1980), Peterson (1990), Church and Jones (1995), Mitchell (2006), Zaitsev *et al*. (2008*a*,*b*).
** after Kamenetsky *et al*. (2006).
*** after Gittins and McKie (1980), Peterson (1990), Church and Jones (1995); Dawson *et al*. (1996), Zaitsev *et al*. (2008*a*).

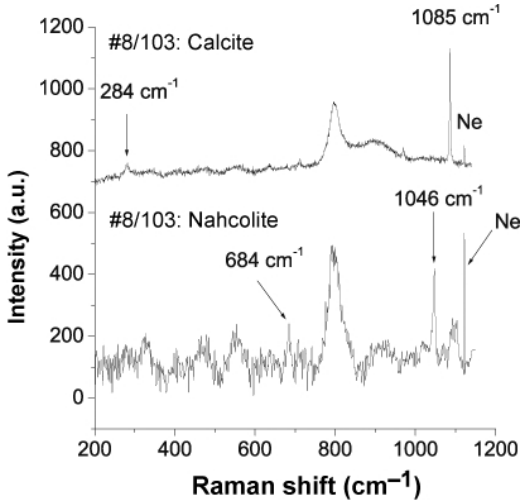

FIG. 6. Raman spectra of nahcolite and calcite microcrystals in diamond crystal #8/103. The characteristic Raman bands for nahcolite and calcite are 1046 and 1085 cm^{-1} respectively. For nahcolite, the weak line at 684 cm^{-1} is also characteristic. The sharp line at 1122.5 cm^{-1} (Ne) is a neon line in the spectrum and can be used for calibration. The broad band at about 800 cm^{-1} results from the diamond host. The high background in the calcite spectrum was not subtracted.

portion of the diamond. They are well formed, prism-bipyramidal crystals, 10–30 mm in size.

The calcite inclusion from foil #1734 is essentially $CaCO_3$ (Ca = 99.26 at.%), with a minor admixture of Sr (0.74 at.%) and trace contents of Ba.

Ferropericlase-periclase and wüstite-magnesiowüstite

Several inclusions (foils ##1625, 1671 and 1734) contain small (<100 nm) nano-inclusions of magnesiowüstite which is the most common mineral inclusion for the Juina diamonds. These inclusions were studied in detail in foil #1625. They are euhedral (octahedral and cubic-octahedral), slightly rounded grains of wüstite-magnesio-wüstite and periclase-ferropericlase, with grain sizes in the range of several nanometres up to 100 nm, embedded in a porous, amorphous, carbonate matrix (Fig. 7*a*). Under TEM examination, the matrix material does not display diffraction contrast during tilting of the sample, and electron diffraction confirms its amorphous state. An EDX-analysis of the matrix reveals that it is composed mainly of Ca, C, and O, with minor Fe and Ga; this suggests its carbonate composition. The amorphous state of the carbonate is likely an artifact caused by Ga-ion implantation during FIB milling.

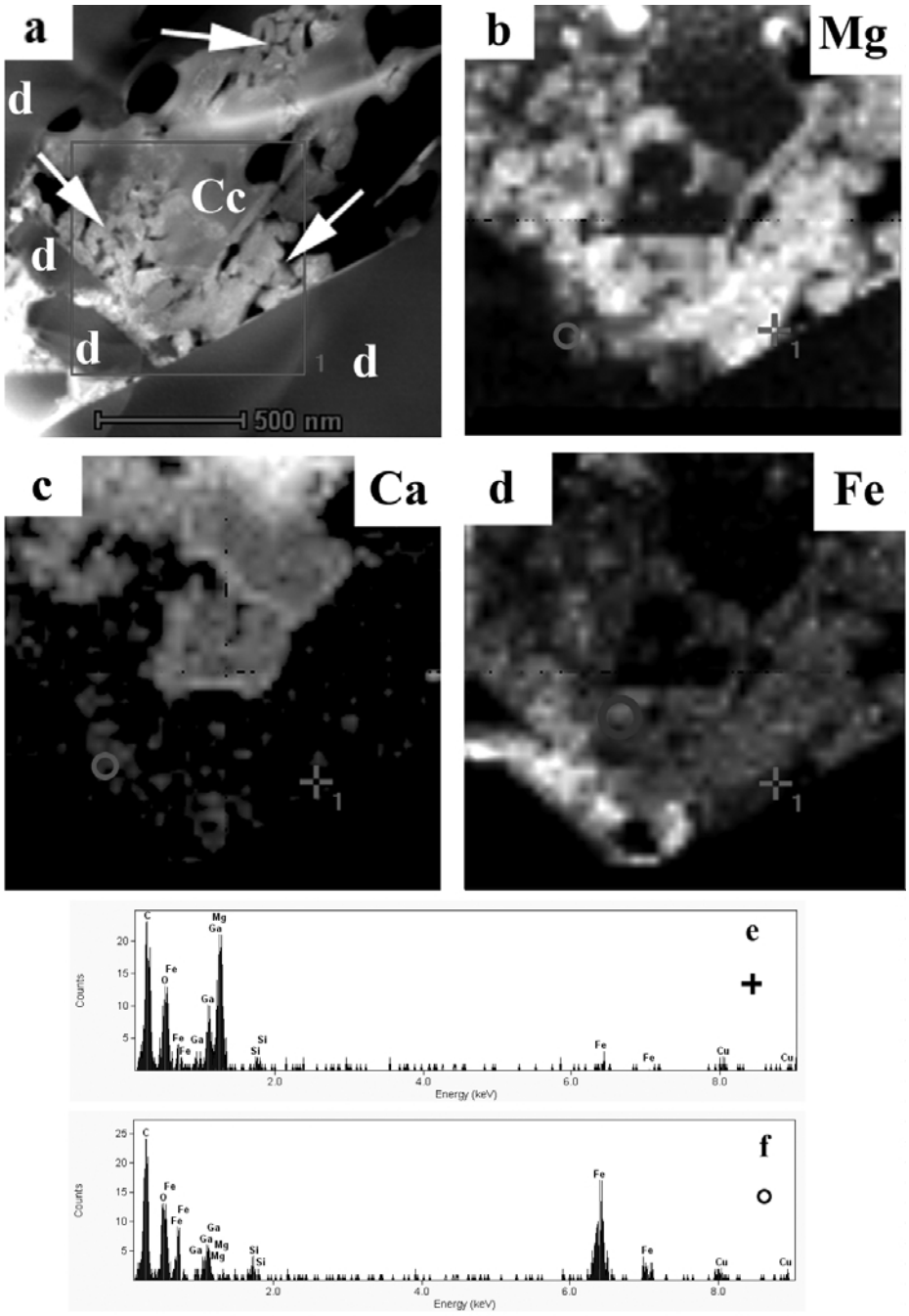

FIG. 7. Inclusion in diamond composed of ferropericlase, wüstite and Mg-wüstite in a carbonate matrix; foil #1625. (*a*) High-angle annular dark-field (HAADF) image of the inclusion. Diamond is labelled as 'd'. White arrows point to crystals of Mg-wüstite and ferropericlase. A square defines the area for the element maps. (*b*–*d*) High-resolution element maps using Mg-*K*α, Ca-*K*α and Fe-*K*α X-ray intensity. Tiny grains of wüstite are visible within Mg-wüstite and ferropericlase. Circle (○) and cross ($+_1$) indicate the positions where the chemical compositions, displayed in figures (*e*) and (*f*), have been acquired.

The nano-crystals embedded in the carbonate matrix exhibit diffraction contrast and electron diffraction provides evidence of a crystalline state. However, some amorphous material is also present between the grains and at triple junctions. This material is composed of SiO_2 plus amorphous carbon.

Several individual nanometre-sized crystalline inclusions were analysed by EDX-analysis. The grains are composed of Mg, Mn, Fe, and O. The chemical composition of most of the nanocrystals varies within the following range (in at.%): Mg = 84.9−92.1; Mn = 0.2−1.2; Fe = 6.9−14.9 (Table 5).

High-resolution lattice fringe images from some of the analysed nanocrystals were acquired. FFT of the lattice fringe images result in diffraction patterns. Different *d*-spacing values were measured from these diffraction patterns. One FFT-derived diffraction pattern with the zone axis [01$\bar{1}$] was completely indexed, and the grain identified as ferropericlase. The angles measured between adjacent planes are: (200):(111) = 54º, (111):($\bar{1}$11) = 70.3º. Based on a cubic structure (NaCl) for the mineral, the calculated angles between these planes are: (200):(111) = 54.7º and (111):($\bar{1}$11) = 70.53º. These are in very good agreement with the observed angles, and serve as strong evidence for a cubic (NaCl) structure for the ferropericlase nano-crystals. Three characteristic sets of *d*-spacing values from seven different nanocrystals were calculated: 0.2457 nm (σ = 0.0090); 0.2148 nm (σ = 0.0018); and 0.1493 nm (σ = 0.0015). The measured *d* spacings can be indexed as ferropericlase (111) 0.246 nm, (200) 0.215 nm, and (202) 0.148 nm. The calculated unit-cell parameter a_0 from the *d*-spacing values is 0.4249 nm (σ = 0.0058) and fits the data (a_0 = 0.4237 nm, at ambient conditions) given in Dubrovinsky *et al*. (2001). Based on the chemical composition obtained and the observed lattice parameters, the nanocrystals are ferropericlase.

TABLE 5. Chemical composition of wüstite and periclase inclusions in diamond #8/103 (at. %; AEM data).

Grain #	Mg	Mn	Fe	Total
Wüstite				
1	3.4	n.d.	96.6	100.0
2	15.3	0.4	84.3	100.0
3	13.2	n.d.	86.8	100.0
4	13.0	0.6	86.4	100.0
5	1.9	n.d.	98.1	100.0
Periclase				
6	85.4	0.4	14.2	100.0
7	91.2	1.2	7.6	100.0
8	85.5	0.4	14.1	100.0
9	92.1	1.0	6.9	100.0
10	87.7	1.2	11.1	100.0
11	85.5	0.5	14.0	100.0
12	84.9	0.2	14.9	100.0
13	86.7	0.9	12.4	100.0
14	89.7	0.6	9.7	100.0
15	86.4	0.4	13.2	100.0
16	87.8	1.2	11.0	100.0
17	91.3	0.6	8.1	100.0
18	91.5	1.1	7.4	100.0
19	90.3	0.4	9.3	100.0
20	86.8	0.6	12.6	100.0

n.d. = not detected.

Additionally, X-ray intensity element maps provide evidence that some of the small (~20 nm; see Fig. 7*a*) grains present within the studied diamond are highly enriched in iron and strongly depleted in Mg. An EDX spectrum (Fig. 7*f*) shows that these nanocrystals are composed almost exclusively of Fe and O. High-resolution images of the small grains display lattice fringes with *d*-spacing values in accordance with the mineral wüstite: (111) 0.244−0.246 nm observed (0.2498 nm calculated), and (200) 0.206−0.208 nm observed (0.2163 nm calculated). The unit-cell parameter a_0 calculated from the *d* spacings is 0.4192 nm compared with 0.4298 nm (Kondo *et al*., 2004). The analysed grains exhibit some compositional variation, with a magnesium index Mg# ranging from 1.9 to 15.3 (Table 5).

High-resolution element mapping with sample drift correction using the TEM EDX-system resolved details of the chemical composition of the nanocrystals. The C-*K*α, O-*K*α, Mg-*K*α, Ca-*K*α and Fe-*K*α X-ray intensities were utilized for imaging. The data evaluation software (*TIA*) allowed for the extraction of complete EDX spectra from a selected location indicated by the position of the cursor in Fig. 7*b*−*d*. A high-resolution element map shows that Fe within the crystals is inhomogeneously distributed (Fig. 7*d*). The Fe-enriched parts are ~20−40 nm in size and span the compositional range of 33.9−14.5 at.% Fe and 66.1−85.5 at.% Mg; they correspond to wüstite and Mg-wüstite. In contrast, the Mg-rich volumes display a chemical composition of

6.5−12.2 at.% Fe and 93.5−87.8 at.% Mg; they correspond to Fe-periclase and periclase.

Nano-inclusions form two groupings with respect to their Mg index. Most of the grains are highly enriched in Mg with low Fe concentrations (Mg# = 84.9−92.1); these are periclase and Fe-periclase. However, a significant portion of analysed grains (~25%) are low-Mg, high-Fe wüstite with Mg# = 1.9−15.3. A subset of these have an extremely large Fe content (Mg# = 1.9−3.4), close to stoichiometric wüstite.

Wollastonite II (high)

Wollastonite II (high) has previously been identified in our studies of other diamonds from the Rio Soriso placer in Juina; it occurs in association with calcite and cuspidine (Wirth *et al*., 2009). In the studied diamond (foil #1734), nano-inclusions of wollastonite II (high) were identified within the calcite matrix, along with nyerereite, Ca-garnet, apatite and Mg-wüstite (?). It forms several near-euhedral grains, some of them approximately 500 nm in size (Fig. 2*a*). The chemical composition is (in at.%): Ca = 49.7, Si = 50.1, and Fe = 0.2. The Ca: Si ratio is 0.992.

Wollastonite II (high) was also confirmed from diffraction patterns derived from high-resolution images (FFT). A comparison of the observed angles between the planes and the calculated angles resulted in complete accordance of the angles.

Ca-garnet

In the calcite matrix of an inclusion from foil #1734, at least three grains of Ca-rich garnet (Ca-Ti-Al-Mg-Fe-Zr) were identified, with the largest grain approximately 600 nm × 200 nm in size (Fig. 2*a*,*b*). From that grain, two different diffraction pattern (FFT) of different orientations were acquired and indexed. The calculated angles and *d* spacings indicate the mineral to be kimzeyite, a zirconium-bearing garnet with the unit-cell parameter a_0 = 1.2365 nm (Munno *et al*., 1980), previously identified in carbonatites (e.g. Nickel, 1960). The observed crystallographic data match kimzeyite reasonably well, however, the chemical composition deviates somewhat, particularly with respect to the Zr concentration which is too small for kimzeyite; in our sample, Zr is present only as a minor component. The garnet described here is, most likely, a solid solution in the ternary system between the end members andradite–kimzeyite–schorlomite.

Spinel group

Two types of spinel were distinguished among mineral inclusions in diamond: Mg-Fe (magnesioferrite) and Fe-spinel (magnetite).

Magnesioferrite

Magnesioferrite was identified by FFT in two foils (##1659 and 1673) in association with carbonates (nyerereite and calcite), phlogopite (?) and apatite (foil #1659). It forms several perfect octahedral crystals, 200−700 nm in size (Fig. 3).

In foil #1659, spinel exhibits zoning with respect to Mg and Fe (Table 6). The core of the spinel is Fe-rich (Mg# = 13.5), similar to a previously described spinel included in diamond #8/106 (with a Mg# = 13.3; Wirth *et al*., 2009), while the rim is strongly magnesian (Mg# = 90.8). At the same time, the Cr content remains almost constant (Cr# = 26.6 and 25.0 for core and rim respectively). In contrast to those spinel inclusions present within nyerereite and gregoryite phenocrysts from Oldoinyo Lengai carbonatites, and which belong to the jacobsite series (Mitchell and Belton, 2004), our grains contain only minor Mn and are essentially magnesioferrite.

Magnetite

Magnetite was identified in inclusions from three of the foils, either singly (foil #1622), embedded in the graphite matrix (foil #1658), or in association with calcite (foil #1671). It forms nanocrystals 30−100 nm in size. Magnetite is confirmed (in foil #1622) by *d*-spacing values

TABLE 6. Chemical composition of spinel inclusion in diamond #8/103 (at.%; EDX data).

Element and ratio	— Foil #1659 —	
	Core	Rim
Si	1.8	0.9
Ti	3.2	0
Al	3.3	0.3
Cr	1.2	0.1
Fe	79.0	20.5
Mg	10.9	77.4
Mn	0.6	0.8
Total	100.0	100.0
100Cr/(Cr+Al)	26.6	25.0
Mg# = 100Mg/(Mg+Fe+Mn)	12.0	78.4

measured from high-resolution images (0.244 nm $(222)_{magnetite}$, 0.212 nm $(132)_{magnetite}$) and 0.206 nm $(140)_{magnetite}$. From the EDX spectra, these inclusions also contain minor Al, Si, Ti, Ni and Cr.

Diamond

In a composite inclusion from foil #1734, a single euhedral diamond was identified. It is an octahedral crystal, ~250 nm × 400 nm in size, and is embedded in a matrix of calcite, unconnected to the host diamond (Fig. 2*d*). This diamond exhibits slightly rounded edges, which might indicate resorption in a carbonatitic melt. It has a crystallographic orientation that is entirely different from the host diamond. Dark-field imaging, by means of the (111) host diamond intensity, resulted in a bright contrast of the host diamond and in dark contrast of the included diamond, again demonstrating the discrete nature of the diamond grain.

Other minerals

Olivine was identified in a composite inclusion (in foil #1659) as an elongate, lath-shaped, single crystal ~2 μm × 0.25 μm in size, intergrown with nyerereite (Fig. 3). While the crystal habit is unusual for olivine, its crystal structure as olivine was confirmed by diffraction-pattern characterization (FFT) derived from high-resolution images. We obtained three individual diffraction patterns in 3 different orientations with the zone axes: -[201], $[1\bar{2}2]$ and $[04\bar{1}]$. Measuring the angles between adjacent planes, we found excellent accordance between the calculated angles based on the olivine structure and the measured angles from the diffraction pattern (FFT).

The chemical composition of the olivine is (in at. %): Si = 34.39; Fe = 4.15; Mg = 60.85; and Ca = 0.59; Mg# = 93.6. The formula calculated from the chemical composition is: $(Mg_{1.999}Ca_{0.011}Fe_{0.059})_{2.069}Si_{0.965}O_4$. The lath-shaped morphology might be reasonable if we assume that the olivine was initially ringwoodite or wadsleyite that has transformed retrogressively to olivine.

Phlogopite is present in two inclusions (foils ##1659 and 1673), where it forms small flakes, ~200–350 nm in size. In foil #1659, it is associated with olivine (Fig. 3) and has a chemical composition of (in at.%): Mg = 20.5, Al = 15.3, Si = 53.5, K = 7.6, Fe = 3.1.

Apatite usually forms small (<100 nm), elongated, euhedral grains (Figs 3, 4*c*); in an inclusion from foil #1659, its size reaches ~500 nm. It is always associated with the carbonates nyerereite and calcite. The EDX spectrum for sample #1734 displays elevated concentrations of La, Ce and Nd (<1 at.% each).

Conclusions and discussion

General notes

All mineral inclusions characterized in this work are discrete solid phases, as are their associations. This is important because some uncommon phases, occurring as diamond inclusions (brines, fluorides, etc.), have earlier been reported as part of multi-phase inclusions in diamond, that contain fluid bubbles from which they may have originated; these samples should therefore be considered as inclusions of secondary nature (e.g. Klein-BenDavid *et al*., 2006; Logvinova *et al*., 2008).

In this work (as in our previous article; Wirth *et al*., 2009), we identify and describe single-phase, solid inclusions. Some of the minerals contain nano-sized, irregularly-formed pores (e.g. see Fig. 2), which probably contained fluid that was released during sample preparation. These inclusions are analogous to fluid and melt inclusions in kimberlitic olivine (e.g. Kamenetsky *et al*., 2008).

Most of the described inclusions are nanometre-sized. However, they exceed so-called 'critical nucleus' size (usually at 10–12 nm), i.e. according to classical nucleation theory (CNT), they are thermodynamically stable and grew with the same kinetics as macro-sized mineral phases (Waychunas and Zhang, 2008).

Carbonatitic mineral association in diamond

Most of the mineral phases reported in this work and in our previous publication (Wirth *et al*., 2009) cannot be attributed to any known associations. In contrast to silicates and oxides, which predominate in ultramafic, eclogitic and super-deep parageneses, the newly identified set of inclusions is composed mostly of carbonates and halides along with phosphates, and a minor proportion of oxides, silicates and sulphides.

Single grains of carbonate included in diamond have been reported before (e.g. Sobolev *et al*., 1997); however, they have never previously been used to define a paragenetic association as is described in this work. Only recently, an

association of syngenetic inclusions of calcite and walstromite-structured $CaSiO_3$, both strongly enriched in light *REE*, has been reported in two Juina diamonds (Brenker *et al*., 2007). An association of calcite, together with wollastonite II (high), cuspidine and monticellite, as well as a series of halide and sulphate inclusions, have been identified in other diamonds from the same area (Wirth *et al*., 2009). Table 7 presents a list of these minerals which form an unusual association; almost none have previously been reported in association with diamond. The list includes a series of halides, such as halite, sylvite, hydrophilite and cotunnite which we found in our previous work in association with calcite, wollastonite II, anhydrite, phlogopite, cuspidine, and other minerals (Wirth *et al*., 2009).

It is evident that the bulk of minerals are different carbonate-mineral species (Sr- and Ba-bearing calcite, nyerereite, nahcolite) and halides (halite, sylvite, hydrophilite, cotunnite), with an admixture of apatite enriched in *REE* (La, Ce, Nd), oxides and silicates. Such mineral associations are characteristic of only two principal rock types, (1) carbonatites (more precisely, natrocarbonatites) (e.g. Peterson, 1990; Dawson, 1993), and (2) chloride-carbonate inclusions in kimberlites (e.g. Kamenetsky *et al*., 2004; Sharygin *et al*., 2008). Hence, these may be called a carbonatitic-type mineral association, or, in this case, natrocarbonatitic association. We suggest that the list of minerals of this association, presented in Table 7, is far from complete, and may be extended with future research.

A close ('touching') assemblage of calcite with walstromite-structured $CaSiO_3$ and $CaTiO_3$ (Brenker *et al*., 2007) and ferropericlase (this work) indicates an origin of the carbonatitic-type association in the lower mantle, below the 660-km discontinuity. There are lower-pressure phases in the carbonatitic association, such as olivine, wollastonite, and a few others. It may be suggested that such assemblages are retrograde phase transformations of MgO and Mg-Si 'perovskite' (to olivine) and Ca-Si 'perovskite' (to wollastonite-II). On the other hand, some of the observed minerals (wüstite with Mg# = 1.9–15.3) may have formed as deep as the lowermost mantle (see next section).

Although some of the minerals described in this work and also by Wirth *et al*. (2009) have been reported earlier by Klein-BenDavid *et al*. (2006) in diamonds from Diavik mine, Canada (sylvite in association with carbonates of variable composition, apatite, and mica) and by Logvinova *et al*. (2008) in diamonds from Siberian mines (sylvite), there are significant differences in their occurrence and paragenesis. These earlier reported diamonds are from 'common' deposits originating in the upper mantle and belonging to the ultramafic association. The 'uncommon' carbonates and halides, in these diamonds, are not single, solid phases, they are parts of multi-phase assemblages which include both solid and fluid phases (bubbles). These multi-phase inclusions, most probably, were initially fluid inclusions of carbonate or chloride-carbonate and silicate composition, trapped by diamonds from the media from which the diamonds originated, and partly crystallized during the course of ascent to the Earth's surface in proto-kimberlitic magma, i.e. they are of secondary origin.

Wüstite inclusions: material from the Earth's lowermost mantle?

Among the lower-mantle inclusions, ferropericlase predominates in association with Mg-Si, Ca-Si and Ca-Ti perovskite, stishovite, and other minerals. Models proposing a homogeneous mantle suggest a constant, basically magnesian composition for these minerals, with Mg# in the range of 87–93 (e.g. Fiquet *et al*., 2008). However, ferropericlase inclusions from different regions have a Mg# index that varies from 38 (magnesiowüstite) to 94 (almost pure periclase) (e.g. Kaminsky *et al*., 2001). One magnesiowüstite grain identified in a diamond from Monastery, South Africa in the 1980s reportedly had a Mg# of 12 (Moore and Gurney, 1989). Recently, an unusual pure wüstite inclusion was recorded in one of the diamond crystals from the Los Coquitos area, Venezuela. It has an FeO content of 97 wt.%, with only 0.09 wt.% MgO, and Mg# = 0.2. It has been suggested that this wüstite might belong to the lowermost mantle (Kaminsky *et al*., 2006). The present study has identified other wüstite inclusions in diamond from the Juina area, Brazil. These findings contradict the homogeneous mantle model.

A heterogeneous lower mantle model explains geophysical features present beneath different regions more effectively than a homogeneous mantle model. It has been suggested that, in the lowermost mantle, high-density Fe-rich wüstite may occur (Badro *et al*., 2003). High-pressure experiments confirmed this suggestion. Dubrovinsky *et al*. (2001) demonstrated that

TABLE 7. Mineral inclusions in diamond of carbonatitic paragenetic association type.

Mineral	Index	Formula	Association	Reference; (Sample)
Carbonates				
Calcite	Cc	$CaCO_3$	Phl	Sobolev *et al.* (1997)
			CaSiPvk+CaTiPvk+Ol	Brenker *et al.* (2007)
			Mont+Wo II+Cusp	Wirth *et al.* (2009); (8/104-1)
			Per+Wu	This work; (8/103)
			Sp+Ap	
			Sp+Phl(?)	
			Nyer+Wo II+CaGa	
			Nah+Phl	This work; (8/103-2)
Dolomite	Dol	$CaMg(CO_3)_2$	Ilm	Wirth *et al.* (2009); (8/106)
			Sp+Phl	
Nyerereite	Nyer	$(Na,K)_2Ca(CO_3)_2$	Cc+Wo II+CaGa+Ap+MgWu(?)	This work; (8/103)
			Ol+Sp+Ap+Phl(?)	
Nahcolite	Nah	$NaHCO_3$	Cc+Phl	This work; (8/103-2)
Halides				
Halite	Ha	NaCl	Coes+Sy+Hy+Cot+PbO_2+TiO_2+Anh	Wirth *et al.* (2009); (8/105)
Sylvite	Sy	KCl	Coes+Ha+Hy+Cot+PbO_2+TiO_2+Anh	
Hydrophilite	Hy	$CaCl_2$	Coes+Ha+Sy+Cot+PbO_2+TiO_2+Anh	
Cotunnite	Cot	$PbCl_2$	Coes+Ha+Sy+Hy+PbO_2+TiO_2+Anh	
Sulphates				
Anhydrite	Anh	$CaSO_4$	Coes+Ha+Sy+Hy+Cot+PbO_2+TiO_2	Wirth *et al.* (2009); (8/105)
Phosphates				
Apatite	Ap	$Ca_5[PO_4]_3(F,Cl)$	Nyer+Ol+Sp+Phl(?)	This work; (8/103)
			Nyer+Cc+Wo II+MgWu(?)	
			Cc+Sp+MgWu	
Oxides				
Coesite	Coes	SiO_2	Ha+Sy+Hy+Cot+PbO_2+TiO_2+Anh	Wirth *et al.*, 2009; (8/105)
Rutile(?) (α-PbO_2 structure)	Ru(?)	TiO_2	Coes+Ha+Sy+Hy+Cot+Plat+Anh	Wirth *et al.* (2009); (8/105)
Plattnerite	Plat	PbO_2	Coes+Ha+Sy+Hy+Cot+Ru+Anh	Wirth *et al.* (2009); (8/105)
Periclase (incl. FePer)	Per	MgO	Cc+Wu	This work; (8/103)

Wüstite (incl. MgWu)	Wu	FeO	Cc+Per	This work; (8/103)
			Cc+Sp+Ap	
			Nyer+Cc+Ap+Wo II	
Spinel-magnesioferrite	Sp	$(Mg,Fe)(Al,Fe)l_2O_4$	Dol+Phl+Ilm	Wirth *et al.* (2009); (8/106)
			Nyer+Ol+Ap+Phl(?)	This work; (8/103)
			Cc+Phl(?)	
Spinel-magnetite	Sp	Fe_3O_4	Cc+Ap	This work; (8/103)
Ilmenite	Ilm	$FeTiO_3$	Dol	Wirth *et al.* (2009); (8/106)
			Sp+Phl	
CaSi-perovskite	CaSiPvk	$CaSiO_3$	Cc+Ol+CaTiPvk	Brenker *et al.*, (2007)
CaTi-perovskite	CaTiPvk	$CaTiO_3$	Cc+Ol+CaSiPvk	Brenker *et al.* (2007)
Silicates				
Olivine	Ol	$(Mg,Fe)_2SiO_4$	$Cc+CaSiO_3+CaTiO_3$	Brenker *et al.* (2007)
			Nyer+Sp+Ap+Phl(?)	This work; (8/103)
Monticellite	Mont	$CaMgSiO_4$	Cc+Wo II+Cusp	Wirth *et al.* (2009); (8/104-1)
Wollastonite-II (high)	Wo II	$CaSiO_3$	Cc+Cusp+Mont	Wirth *et al.* (2009); (8/104-1)
			Cc+Nyer+CaGa+Ap+MgWu	This work; (8/103)
Ca-Garnet	CaGa	$Ca_3(Fe,Zr,Ti)_2[(Si,Al)O_4]_3$	Cc+Nyer+Wo II+Ap+MgWu	This work; (8/103)
Phlogopite	Phl	$KMg_3[Si_3AlO_{10}](F,OH)_2$	Cc	Sobolev *et al.* (1997)
			Dol+Ilm+Sp	Wirth *et al.* (2009); (8/106)
			Nyer+Ol+Sp+Ap	This work; (8/103)
			Cc+Sp	
			Nah+Cc	This work; (8/103-2)
Cuspidine	Cusp	$Ca_4[Si_2O_7](F,OH)_2$	Cc+Wo II+Mont	Wirth *et al.* (2009); (8/104-1)
Sulphides				
Fe-Ni-Cu sulphide	Sulph		(Cc+Wo II+Cusp+Mont)	Wirth *et al.* (2009); (8/104-2)

ferropericlase under pressures >85 GPa and high temperatures may dissociate into Mg-rich and Fe-rich oxide components. Recent experiments, carried out at the GFZ Research Centre in Potsdam at 80 GPa, demonstrated that heating of the layered system MgO-$CaCO_3$-FeO-$CaCO_3$-Mg above the melting temperature of Fe produced ferropericlase and Mg-wüstite, and that in amorphous carbonate, small crystals of diamond grew (S. Speziale, pers. comm.).

The discovery of highly Fe-rich wüstite as inclusions in lower-mantle diamonds from three different locations, South Africa, Venezuela and Brazil supports both experimental data and geophysical observation, and confirms the concept of a heterogeneous lower mantle, which includes not only a deep-mantle perovskite/post-perovskite phase change, but layering, partial melting and small-scale convection at the base of the lower mantle.

Lower-mantle carbonatitic magma

In contrast to hypotheses invoking low-pressure unmixing of carbonatites from associated alkaline igneous magmas, other hypotheses propose that carbonatites are primary, mantle-derived melts (e.g. Harmer and Gittins, 1998). The carbonatitic mineral association in diamond described above is considered as direct evidence for such carbonatitic magma formed at depths of greater than the 660 km discontinuity and possibly as deep as the lowermost mantle.

These data agree well with the numerous observations of carbonate melt inclusions and chloride-carbonate brine inclusions in Siberian, African, Indian, Canadian and Brazilian diamonds (e.g. Izraeli *et al*., 2001). The compositional variations of these inclusions demonstrate the existence of two separate trends among initial melts, a silicate-carbonate melt and carbonate-chloride melt (Navon *et al*., 2003).

Safonov *et al*. (2007) proved experimentally the existence of both carbonate-silicate and chloride-carbonate immiscible melts, which are similar to the melt and brine inclusions in natural diamonds in chloride-carbonate-silicate systems at 5 GPa pressure and at temperatures of 1400–1600ºC. More recent experiments, performed by Litasov and Ohtani (2009) for the peridotite-carbonate-silicate system at higher pressures, corresponding to the transition zone and upper part of the lower mantle (7.0–16.5 GPa) and temperatures (up to 1800ºC), confirmed this model and demonstrated that evolution of homogeneous Cl-bearing silicate melt may produce immiscible Si-poor carbonatite and chloride-carbonatite melts.

Subduction or primary magmatic?

One overriding question must be raised. Is the carbonatitic magma, which produced diamond and carbonatitic-type mineral inclusions, indeed primary, primitive magma *sensu stricto*, or has it originated as a result of subduction processes (i.e. it is recycled from other rocks)?

Brenker *et al*. (2007) suggested the possibility of forming a carbonate reservoir as a result of subduction of CO_2-enriched crustal material to great depths in the lower part of the transition zone (580 km depth) or even in the lower mantle. Developing this idea, Walter *et al*. (2008) envisaged the existence of a carbonatitic magma at the depth of the transition zone. Based on calculations of incompatible trace element abundances for a melt coexisting with Ca-Ti-Si perovskite (as is present in inclusions in Juina diamonds), Walter *et al*. (2008) proposed that deep, low-degree partial melting of subducted, carbonated, oceanic crust resulted in the production of trace-element-enriched, carbonatite melts.

These conclusions agree with the encapsulating of 'unusual' inclusions (halides, anhydrite, cuspidine etc.) in a diamond with a light C isotopic composition (i.e. with $\delta^{13}C$ from −14 to −25‰ V-PDB) and their paragenetic ('touching') association with coesite (Wirth *et al*., 2009). However, the inclusions reported in the present work (nyerereite, Ba-Sr calcite and others) are encapsulated, not in a subduction-type diamond, but in a typical 'superdeep' diamond of type II, with presence of only B-centres (N_B) and a total N concentration of 44 ppm, and with an anomalously large concentration of hydrogen (C–H) centres. This is characteristic of 'juvenile' lower-mantle diamonds, and gives a basis for a conclusion on the existence of juvenile, magmatic, carbonatitic magma at that depth.

According to recent high-pressure experimental data, a variety of carbonatitic melts were produced by partial melting of chloride-carbonate peridotite (Litasov and Ohtani, 2009). The chloride/carbonate ratio in the chloride-carbonate liquid and composition of the interacting silicate assemblage produces a wide range of the chloride-rich carbonate-silicate melts (Safonov *et al*., 2009). A great compositional variety of

melt inclusions in diamond and experimental data give reason to suggest a polygenetic nature for primitive carbonatitic magmas.

Volatiles and their role in diamond formation

According to experimental data, Cl and F are of great importance in the formation of diamond (e.g. Pal'yanov *et al.*, 2007). The exact concentration of volatiles in initial, diamond-forming, carbonatitic magmas remains unknown; however, estimates are high. Burgess and Turner (1995) estimated the Cl content in mantle-derived fluid at 2–5 wt.%, which is in a good agreement with compositions of natrocarbonatitic lavas and carbonate melt inclusions in diamonds. The observations on carbonatitic eruptions of Oldoinyo Lengai in the 1980s demonstrated that carbonatitic magma, during the course of its evolution, can be enriched in Cl, F and Ba, whose concentrations increase with the evolution of the magma: Cl from 1.5 to 5.5 wt.%; F from 1 to 6 wt.%; BaO from 1 to 2.5 wt.% (Gittins and Jago, 1998). The carbonate-rich inclusions in diamond contain 6–12 wt.% Cl (Klein-BenDavid, 2006).

Another volatile species which probably plays a substantial role in deep magmatism, particularly in terms of diamond formation, is hydrogen. Its structural position, and even its concentration in diamond, are as yet unknown: to date, there are no reliable analytical methods to establish this. The only H-impurity centre, indicated in IR spectra with two absorption peaks, at 3107 and 1405 cm^{-1}, has been attributed to C–H bond vibrations (e.g. Woods and Collins, 1983). The H centre has been identified in diamonds infrequently; usually its intensity (which is considered as a relative value) does not exceed 0.1–0.3 cm^{-1}; the strongest absorption detected at 3107 cm^{-1} has been 12.8 cm^{-1} (Woods and Collins, 1983). In contrast to most diamond deposits worldwide, almost all diamonds from the Juina pipes (80–89 %) have noticeable (up to 4.2 cm^{-1}) absorption levels of the hydrogen C–H centre (Kaminsky *et al*., 2009*a*). Further evidence for a large concentration of H in diamond-producing carbonatitic magma is the presence of H-containing nahcolite inclusions in diamond.

Formation of diamond

According to experiments in the alkaline carbonate–C and carbonate–fluid–C systems at 5.7–7.0 GPa and at 1150–1700ºC performed by Pal'yanov *et al*. (2002), only alkaline carbonate melts and C-O-H fluid can provide diamond crystallization from a melt at the *P-T* conditions corresponding to the formation of natural diamonds. Furthermore, the most likely medium for the nucleation and growth of diamond in nature is fluid-bearing alkaline carbonate melts. Recent experiments by Shatskiy *et al*. (2008) confirmed that at 6.3 GPa, in the systems K_2CO_3-SiO_2-C and K_2CO_3-Mg_2SiO_4-C, the field of diamond nucleation is limited by not less than 75–80 wt.% of carbonate component, when silica is completely dissolved in the carbonate melt. As the silicate content increases, the carbonate-silicate melt increases its polymerization and viscosity, and ceases to provide spontaneous nucleation of diamond. In the domain of large concentrations of silicate, only seeded diamond growth and recrystallization of metastable graphite are possible. Litvin *et al*. (2008) studied diamond crystallization experimentally at 8.5 GPa in C-bearing melts corresponding to mixtures of model eclogite with dolomite, K_2CO_3, and multi-component K-Na-Ca-Mg-Fe carbonatites. The concentration barriers of diamond nucleation were determined for these melts as 35, 65, and 40 wt.% of the silicate components respectively. At higher contents of silicate components, diamond may grow only on seeds simultaneously with the nucleation of thermodynamically unstable graphite. These data demonstrate persuasively crystallization of diamond from magmatic, predominantly carbonatitic melt. Litasov and Ohtani (2009) reported the presence of micro-diamonds among the run products (forsterite, enstatite, garnet) in their experiments at pressures of 7.0–16.5 GPa, corresponding to the transition zone and the uppermost lower mantle. A nano-diamond, identified in this work in foil #1734, is fully embedded in a calcite matrix, and may be considered as a natural example of such process.

Such mechanisms can be realized in natural systems for crystallization of diamond directly from a lower-mantle carbonatitic magma. For the carbonate-containing oceanic plates subducted to the lower mantle, crystallization of diamond may be suggested, either from a secondary carbonatitic melt, formed at subducted, carbonated oceanic crust (Walter *et al*., 2008), or by an alternative mechanism proposed by Seto *et al*. (2008), which is based on experiments at 30–80 GPa pressure (corresponding to the depth within the Earth of ~800–2200 km) and 1600–3200 K. According to

this mechanism, carbonate decomposes into an assemblage of CO_2 + perovskite in a reaction: $(CaMg)CO_{3(Carb)} + SiO_{2(St)} \rightarrow (CaMg)SiO_{3(Per)} + CO_2$; and furthermore, CO_2 breaks down to diamond and oxygen under geotherm conditions of >70 GPa.

Petrological data indicate that at least some diamonds have a metasomatic origin from C-oversaturated fluids. Numerous finds are known of saline or hydrous-saline, high-density fluids (HDF), rich in volatiles and incompatible elements, included in diamonds (e.g. Navon, 1999; Izraeli *et al*., 2001; Klein-BenDavid *et al*., 2006; Litvin, 2007, Logvinova *et al*., 2008).

Based on our observations and intepretations of mineral inclusions in diamond of carbonatitic association, in both subducted lithosphere (Wirth *et al*., 2009) and juvenile mantle (this work), we suggest that both models can be applied to the natural formation of diamond. In the case of inclusions described in this work, crystallization of multi-mineral associations is most likely from a carbonatitic melt.

Acknowledgements

The authors are grateful to Prof. J.B. Dawson and Prof. R. Mitchell for their careful, constructive reviewing the manuscript; their recommendations helped in improving the paper; to Dr O. Safonov for supplying us with a preprint of his unpublished article; and to Dr Ian Coulson for his help with editing the English.

References

Badro, J., Fiquet, G., Guyot, F., Rueff, J.-P., Struzhkin, V.V., Vanko, G. and Monaco, G. (2003) Iron partitioning in Earth's mantle; toward a deep lower mantle discontinuity. *Science*, **300**, 789–791.

Brenker, F.E., Vollmer, C., Vincze, L., Vekemans, B., Szymanski, A., Janssens, K., Szaloki, I., Nasdala, L. and Kaminsky, F. (2007) Carbonates from the lower part of transition zone or even the lower mantle. *Earth and Planetary Science Letters*, **260**, 1–9.

Burgess, R. and Turner, G. (1995) Halogen geochemistry of mantle fluids in diamonds. Pp. 91–98 in: *Volatiles in the Earth and Solar system* (K.A. Farley, editor). Proceedings AIP Conference, **341**.

Church, A.A. and Jones, A.P. (1995) Silicate-carbonate immiscibility at Oldoinyo Lengai. *Journal of Petrology*, **36**, 869–889.

Dawson, J.B. (1962) The geology of Oldoinyo Lengai. *Bulletin Volcanologique*, **24**, 349–387.

Dawson, J.B. (1993) A supposed sövite from Oldoinyo Lengai, Tanzania: result of extreme alteration of alkali carbonatite lava. *Mineralogical Magazine*, **57**, 93–101.

Dawson, J.B., Pyle, D.M. and Pinkerton, H. (1996) Evolution of natrocarbonatite from a wollastonite nephelinite parent: evidence from the June, 1993 eruption of Oldoinyo Lengai. *Journal of Geology*, **104**, 41–45.

Dubrovinsky, L.S., Dubrovinskaia, N.A., Annersten, H., Hålenius, E. and Harryson, H. (2001) Stability of $(Mg_{0.5}Fe_{0.5})O$ and $(Mg_{0.8}\ Fe_{0.2})O$ magnesiowüstites in the lower mantle. *European Journal of Mineralogy*, **13**, 857–861.

Egorov, K.N., Ushchapovskaya, Z.F., Kashayev, A.A., Bogdanov, G.V. and Sizykh, Yu, I. (1988) Zemkorite, a new carbonate from kimberlites of Yakutia. *Doklady Akademii Nauk SSSR*, **301**, 188–192.

Fiquet, G., Guyot, F. and Badro, J. (2008) The Earth's Lower Mantle and Core. *Elements*, **4**, 177–182.

Gittins, J. and Harmer, R.E. (1997) Dawson's Oldoinyo Lengai calciocarbonatite; a magmatic sövite or an extremely altered natrocarbonatite? *Mineralogical Magazine*, **61**, 351–355.

Gittins, J. and Jago, B.C. (1998) Differentiation of natrocarbonatite magma at Oldoinyo Lengai volcano, Tanzania. *Mineralogical Magazine*, **62**, 759–768.

Gittins, J. and McKie, D. (1980) Alkalic carbonatite magmas; Oldoinyo Lengai and its wider applicability. *Lithos*, **13**, 213–215.

Harmer, R.E. and Gittins, J. (1998) The case for primary, mantle-derived carbonatite magma. *Journal of Petrology*, **39**, 1895–1903.

Hoshino, K., Nagatomi, A., Watanabe, M., Okudaira, T. and Beppu, Y. (2006) Nahcolite in fluid inclusions from Ryoke metamorphic rocks and its implications for fluid genesis. *Journal of Mineralogical and Petrological Sciences*, **101**, 254–259.

Izraeli, E.S., Harris, J.W. and Navon, O. (2001) Brine inclusions in diamonds: a new upper mantle fluid. *Earth and Planetary Science Letters*, **187**, 323–332.

Kamenetsky, M.B., Sobolev, A.V., Kamenetsky, V.S., Maas, R., Danyushevsky, L.V., Thomas, R., Pokhilenko, N.P. and Sobolev, N.V. (2004) Kimberlite melts rich in alkali chlorides and carbonates: A potent metasomatic agent in the mantle. *Geology*, **32**, 845–848.

Kamenetsky, V.S., Sharygin, V.V., Kamenetsky, M.B. and Golovin, A.V. (2006) Chloride–carbonate nodules in kimberlites from the Udachnaya pipe: alternative approach to the evolution of kimberlite magmas. *Geochemistry International*, **44**, 935-940.

Kamenetsky, V.S., Kamenetsky, M.B., Sobolev, A.V., Golovin, A.V., Demouchy, S., Faure, K., Sharygin,

V.V. and Kuzmin, D.V. (2008) Olivine in the Udachnaya-East kimberlite (Yakutia, Russia): types, compositions and origins. *Journal of Petrology*, **49**, 823–839.

Kaminsky, F.V., Zakharchenko, O.D., Davies, R., Griffin, W.L., Khachatryan-Blinova, G.K. and Shiryaev, A.A. (2001) Superdeep diamonds from the Juina area, Mato Grosso State, Brazil. *Contributions to Mineralogy and Petrology*, **140**, 734–753.

Kaminsky, F.V., Zakharchenko, O.D., Khachatryan, G.K., Griffin, W.L. and Channer, D.M.DeR. (2006) Diamond from the Los Coquitos Area, Bolivar State, Venezuela. *The Canadian Mineralogist*, **44**, 323–340.

Kaminsky, F.V., Khachatryan, G.K., Andreazza, P., Araujo, D. and Griffin, W.L. (2009*a*) Super-deep diamonds from kimberlites in the Juina area, Mato Grosso State, Brazil. *Lithos*, **112(Suppl. 2)**, 833–842.

Kaminsky, F.V., Sablukov, S.M., Belousova, E.A., Andreazza, P., Tremblay, M. and Griffin, W.L. (2009*b*) Kimberlitic sources of super-deep diamonds in the Juina area, Mato Grosso State, Brazil. *Lithos*, DOI: 10.1016/j.lithos.2009.07.012.

Klein-BenDavid, O., Wirth, R. and Navon, O. (2006) TEM imaging and analysis of microinclusions in diamonds: A close look at diamond-growing fluids. *American Mineralogist*, **91**, 353–365.

Kondo, T., Ohtani, E., Hirao, N., Yagi, T. and Kikegawa, T. (2004) Phase transitions of (Mg,Fe)O at megabar pressures. *Physics of the Earth and Planetary Interiors*, **143-144**, 201–213.

Le Bas, M.J. (1981) Carbonatite magmas. *Mineralogical Magazine*, **44**, 133–140.

Litasov, K.D. and Ohtani, E. (2009). Phase relations in the peridotite–carbonate–chloride system at 7.0–16.5 GPa and the role of chlorides in the origin of kimberlite and diamond. *Chemical Geology*, **262**, 29–41.

Litvin, Y.A. (2007) High-pressure mineralogy of diamond genesis. Pp. 83–103 in: *Advances in High-Pressure Mineralogy* (E. Ohtani, editor). Special Paper **421**, Geological Society of America, Boulder, Colorado, USA.

Litvin, Yu.A., Litvin, V.Yu. and Kadik, A.A. (2008) Experimental characterization of diamond crystallization in melts of mantle silicate–carbonate–carbon systems at 7.0–8.5 GPa. *Geochemistry International*, **46**, 531–553.

Logvinova, A.M., Wirth, R., Fedorova, E.N. and Sobolev, N.V. (2008) Nanometre-sized mineral and fluid inclusions in cloudy Siberian diamonds: new insights on diamond formation. *European Journal of Mineralogy*, **20**, 317–331.

McKie, D. and Frankis, E.J. (1976) Nyerereite: A new volcanic carbonate mineral from Oldoinyo Lengai, Tanzania. *Zeitschrift für Kristallographie*, **145**, 73–95.

Mitchell, R.H. (2006) Mineralogy of stalactites formed by subaerial weathering of natrocarbonatite hornitos at Oldoinyo Lengai, Tanzania. *Mineralogical Magazine*, **70**, 437–444.

Mitchell, R.H. and Belton, F. (2004) Niocalite-cuspidine solid solution and manganoan monticellite from natrocarbonatite, Oldoinyo Lengai, Tanzania. *Mineralogical Magazine*, **68**, 787–799.

Moore, R.O. and Gurney, J.J. (1989) Mineral inclusions in diamond from the Monastery kimberlite, South Africa. Pp. 1029–1041 in: *Kimberlites and related rocks* (J. Ross *et al*., editors). Geological Society of Australia Special Publication No. 14, vol. 2. Proceedings of the Fourth International Kimberlite Conference, Perth 1986, Blackwell, Carlton, Australia.

Munno, R., Rossi, G. and Tadini, C. (1980) Crystal chemistry of kimzeyite from Stromboli, Aeolian Islands, Italy. *American Mineralogist*, **65**, 188–191.

Navon, O. (1999) Diamond formation in the Earth's mantle. Pp. 584–604 in: *Proceedings of the VIIth International Kimberlite Conference*, *vol. 2*. Red Roof Design, Cape Town, RSA.

Navon, O., Izraeli, E.S. and Klein-BenDavid, O. (2003) Fluid inclusions in diamonds – the carbonatitic connection. *8th International Kimberlite Conference*, Long Abstract FLA_0107.

Nickel, E.H. (1960) A zirconium-bearing garnet from Oka, Quebec. *The Canadian Mineralogist*, **6**, 549–550.

Pal'yanov, Yu.N., Sokol, A.G., Borzdov, Yu.M. and Khokhryakov, A.F. (2002) Fluid-bearing alkaline carbonate melts as the medium for the formation of diamonds in the Earth's mantle: an experimental study, *Lithos*, **60**, 145–159.

Pal'yanov, Yu.N., Shatsky, V.S., Sobolev, N.V. and Sokol, A.G. (2007) The role of mantle ultrapotassic fluids in diamond formation. *Proceedings of National Academy of Sciences USA*, **104**, 9122–9127.

Parthasarathy, G., Chetty, T.R.K. and Haggerty, S.E. (2002) Thermal stability and spectroscopic studies of zemkorite; a carbonate from the Venkatampalle kimberlite of southern India. *American Mineralogist*, **87**, 1384–1389.

Peterson, T.D. (1990) Petrology of natrocarbonatite. *Contributions to Mineralogy and Petrology*, **105**, 143–155.

Safonov, O.G., Perchuk, L.L. and Litvin, Y.A. (2007) Melting relations in the chloride–carbonate–silicate systems at high-pressure and the model for formation of alkalic diamond–forming liquids in the upper mantle. *Earth and Planetary Science Letters*, **253**, 112–128.

Safonov, O.G., Chertkova, N.V., Perchuk, L.L. and Litvin, Yu.A. (2009) Experimental model for alkalic chloride-rich liquids in the upper mantle. *Lithos*, **112(Suppl. 1)**, 260–273.

Seto, Y., Hamane, D., Nagai, T. and Fujino, K. (2008) Fate of carbonates within oceanic plates subducted to the lower mantle, and a possible mechanism of diamond formation. *Physics and Chemistry of Minerals*, DOI 10.1007/s00269-008-0215-9, 7 pp.

Sharygin, V.V., Kamenetsky, V.S., Kamenetsky, M.B. and Golovin, A.V. (2008) Mineralogy and genesis of kimberlite hosted chloride containing nodules from Udachnaya East pipe, Yakutia, Russia. *9th International Kimberlite Conference*, Extended Abstract No. 9IKC-A-00060, 3 pp.

Shatskiy, A., Borzdov, Yu.M., Sokol, A.G., Katsura, T. and Pal'yanov, Yu.N. (2008) Diamond crystallization in carbonate-silicate systems: implications for natural diamond genesis. *9th International Kimberlite Conference*, Extended Abstract No. 9IKC-A-00408, 3 pp.

Sobolev, N.V., Kaminsky, F.V., Griffin, W.L., Yefimova, E.S., Win, T.T., Ryan, C.G. and Botkunov, A.I. (1997) Mineral inclusions in diamonds from the Sputnik kimberlite pipe, Yakutia. *Lithos*, **39**, 135–157.

Taran, M.N., Kvasnytsya, V.M., Langer, K. and Il'chenko, K.O. (2004) Infrared spectroscopy study of nitrogen centres in microdiamonds from Ukrainian Neogenic placers. *European Journal of Mineralogy*, **18**, 71–81.

Thomas, R., Davidson, P. and Hahn, A. (2008) Ramanite-(Cs) and ramanite-(Rb): New cesium and rubidium pentaborate tetrahydrate minerals identified with Raman spectroscopy. *American Mineralogist*, **93**, 1034–1042.

Walter, M.J., Bulanova, G.P., Armsrong, L.S., Keshav, S., Blundy, J.D., Gudfinnsson, G., Lord, O.T., Lennie, A.R., Clark, S.M., Smith, C.B. and Gobbo, L. (2008) Primary carbonatite melt from deeply subducted oceanic crust. *Nature*, **454**, 622–625.

Waychunas, G.A. and Zhang, H. (2008) Structure, chemistry, and properties of mineral nanoparticles. *Elements*, **4**, 381–388.

Wirth, R. (2004) Focused Ion Beam (FIB): A novel technology for advanced application of micro- and nanoanalysis in geosciences and applied mineralogy. *European Journal of Mineralogy*, **16**, 863–877.

Wirth, R., Vollmer, C., Brenker, F., Matsyuk, S. and Kaminsky, F. (2007) Inclusions of nanocrystalline hydrous aluminium silicate 'Phase Egg' in superdeep diamonds from Juina (Mato Grosso State, Brazil). *Earth and Planetary Science Letters*, **259**, 384–399.

Wirth, R., Kaminsky, F., Matsyuk, S. and Schreiber, A. (2009) Unusual micro- and nano-inclusions in diamonds from the Juina area, Brazil. *Earth and Planetary Science Letters*, **286**, 292–303.

Woods, G.S. and Collins, A.T. (1983) Infrared absorption spectra of hydrogen complexes in Type I diamonds. *Journal of Physics and Chemistry of Solids*, **44**, 471–475.

Zaitsev, A.N. and Chakhmouradian, A.R. (2002) Calcite-amphibole-clinopyroxene rock from the Afrikanda Complex, Kola Peninsula, Russia; mineralogy and a possible link to carbonatites; II, Oxysalt minerals. *The Canadian Mineralogist*, **40**, 103–120.

Zaitsev, A.N., Keller, J., Spratt, J., Djefries, T.E. and Sharygin, V.V. (2008*a*) Chemical composition of nyerereite and gregoryite from natrocarbonatites of Oldoinyo Lengai volcano, Tanzania. *Zapiski Vserossiyskogo Mineralogicheskogo Obshchestva (Proceedings of the Russian Mineralogical Society)*, **137(4)**, 101–111. (in Russian).

Zaitsev, A.N., Keller, J., Spratt, J., Perova, E.N. and Kearsley, A. (2008*b*) Nyerereite – pirssonite – calcite – shortite relationships in altered natrocarbonatites, Oldoinyo Lengai, Tanzania. *The Canadian Mineralogist*, **46**, 843–860.